

HORIZON EUROPE PROGRAMME
HORIZON-CL4-2023-DIGITAL-EMERGING-01-33

GA No. 101135196

Developing New 2D Materials and Heterostructures for Printed Digital Devices



2D-PRINTABLE - Deliverable report

D3.2 – Cross-linking forming networks and heterostructures



Funded by
the European Union

Deliverable No.	D3.2	
Related WP	WP 3	
Deliverable Title	Cross-linking forming networks and heterostructures	
Deliverable Date	2025-03-31	
Deliverable Type	REPORT	
Dissemination level	Public (PU)	
Author(s)	Antonio Gaetano Ricciardulli (UNISTRA) Paolo Samorì (UNISTRA)	2025-03-04
Checked by	Jonathan Coleman (TCD)	2025-03-06
Reviewed by	Jonathan Coleman (TCD)	2025-03-06
Approved by	Jonathan Coleman (TCD) - Project Coordinator	2025-03-06
Status	Draft v1.1	2025-03-04

Document History

Version	Date	Editing done by	Remarks
V1.0	2025-03-04	Antonio Gaetano Ricciardulli	
V1.1	2025-03-04	Paolo Samorì	
V2.0			
FINAL			

Project Scientific Abstract

The 2D-PRINTABLE project aims to integrate sustainable large-scale liquid exfoliation techniques with theoretical modelling to efficiently produce a wide range of new 2D materials (2DMs), including conducting, semiconducting, and insulating nanosheets. The focus includes developing the printing and liquid phase deposition methods required to fabricate networks and multicomponent heterostructures, featuring layer-by-layer assembly of nanometer-thick 2DMs into ordered multilayers. The goal is to optimize these printed networks and heterostructures for digital systems, unlocking new properties and functionalities. The project also seeks to demonstrate various printed digital devices, including proof-of-principle, first-time demonstration of all-printed, all-nanosheet, heterostack light-emitting diodes (LEDs). In conclusion, 2D-PRINTABLE will prove 2D materials to be an indispensable material class in the field of printed electronics, capable of producing far-beyond-state-of-the-art devices that can act as a platform for the next generation of printed digital applications.

Public summary

The report outlines the progress in the formation of networks and heterostructures of two-dimensional (2D) materials using cross-linking. To fabricate solution-processed large-area networks and heterostructures, a strategy based on defect-engineering of liquid-phase exfoliated nanosheets to control the selective bridging of adjacent 2D transition metal dichalcogenides (TMDs) flakes of different chemical with molecular linkers has been developed. The major achievements of the deliverable D3.2 reported in this document are:

- **Design of a stepwise microfluidic strategy** to fabricate hetero-networks of 2D TMDs (i.e. MoS₂ and WS₂ as 2D building units). To enable selective cross-linking, cyclic and sequential deposition of MoS₂, π -conjugated dithiolated organic moieties and WS₂ has been developed. The use of π -conjugated dithiolated molecules enables the synergistic bridging of TMDs flakes through their sulfur vacancies, mainly located at the edges of MoS₂ and WS₂ flakes, and creation of further percolation pathways across the network.
- **Spectroscopical and electrical characterization** of the synthesized solution-processed hetero-networks to investigate the characteristic features of such architectures for (opto)electronic devices. Transient absorption spectroscopy (TAS) analysis of MoS₂-WS₂ cross-linked networks revealed unique characteristics beyond the conventional TMD blends. Electrical characteristics of field-effect transistors (FETs) of films based on the hetero-networks indicated improved performances compared to pristine materials.

The work described in this report offers innovative solutions for large-area hetero-networks with tailored properties beyond state-of-the-art (opto)electronics.

Contents

1	Introduction.....	6
2	Methods and core part of the report.....	7
2.1	Background.....	7
2.2	Procedures.....	7
2.3	Data Analysis	8
3	Results & Discussion.....	9
3.1	Results	9
3.2	Contribution to project (linked) Objectives.....	13
3.3	Contribution to major project exploitable result.....	13
4	Conclusion and Recommendation	14
5	Risks and interconnections.....	15
5.1	Risks/problems encountered	15
5.2	Interconnections with other deliverables	15
6	Deviations from Annex 1	16
7	References.....	17
	Acknowledgement.....	18
	Appendix A - Quality Assurance Review Form	Error! Bookmark not defined.

List of Figures

Figure 1. Microfluidic-assisted synthesis

Figure 2. Network imaging

Figure 3. EIS tracking over the film growth

Figure 4. TAS analysis

Figure 5. Electrical characteristics

List of Tables

Table 1. Summary of fits of kinetic traces

Table 2. Mean values and standard deviation of key parameters calculated from the FETs based on BDT networks

Abbreviations & Definitions

Abbreviation	Explanation
2DM	Two-dimensional material
APTES	(3-Aminopropyl)triethoxysilane
BDT	1,4-benzenedithiol
EIS	Electrochemical impedance spectroscopy
R_{ct}	Charge transfer resistance
IPA	Isopropanol
LPE	Liquid-phase exfoliation
NMP	N-Methyl-2-pyrrolidone
SEM	Scanning electron microscopy
AFM	Atomic force microscopy
XPS	X-ray photoelectron spectroscopy
TAS	Transient absorption spectroscopy
FET	Field-effect transistor
μ_{FE}	Field-effect mobility
V_{th}	Threshold voltage
SS	Subthreshold swing
D_{it}	Trap density

1 Introduction

The deliverable D3.2 “Cross-linking forming networks and heterostructures” focuses on the development of novel strategies to form networks of nanosheets synthesized in Work Package 1 (WP1) and the investigation of physical, optical and electrical properties of the newly synthesized cross-linked heterostructures. Defect-engineering offers a versatile approach to build such architectures.^[1] For instance, edge-chalcogen vacancies, which represent the most abundant defects in TMDs, can be exploited as reactive sites to covalently bridge adjacent flakes with molecules with *ad-hoc* functionalities. Nevertheless, to enable cross-linking of LPE nanosheets, processes that allow selective functionalization and formation of controlled heterostructures in terms of componential selectivity are needed. To this end, the microfluidic strategy adopted to build discrete assemblies of 2DMs, as discussed in the report of D2.3, has been adapted and tailored to fabricate large-area solution-processed TMD-based hetero-network displaying properties well beyond those of the individual components. Thus, to form proof-of-concept defect-engineered heterostructures, cyclic and sequential deposition of MoS₂, π -conjugated dithiolated organic moieties and WS₂ have been adopted. Noteworthy, the use of π -conjugated molecular bidentate systems synergistically heals sulfur vacancies in TMDs and generates percolation pathways for enhanced charge transfer among nanosheets, improving the inter-flake electronic connectivity across the network.^[2] The growth of large-area networks has been monitored through the interplay of electron microscopy and *in-situ* electrochemical impedance spectroscopy, providing key insights for WPs beyond WP3, such as WP2 and WP4.

The synthesized cross-linked hetero-networks have been further characterized by TAS, shedding light on the unique optical characteristics of covalently interconnected networks, such as the suppression of the formation of typical tightly bound interlayer excitons of conventional TMD blends, which promotes faster charge separation. These findings open new possibilities for dedicated tasks on the fabrication of stacked heterostructures by printing (i.e. Tasks 3.4, 3.5).

Moreover, to benchmark the objectives of WP3, electrical characterization of FETs based on the synthesized solution-processed heterostructures has been carried out.

2 Methods and core part of the report

2.1 Background

To form cross-linked hetero-networks, inks of LPE MoS₂ and WS₂ were used. As chalcogen vacancies represent the most abundant defects in LPE TMDs (i.e. edge-sulfur vacancies in MoS₂ and WS₂), 1,4-benzenedithiol (BDT) was employed as molecular linker to bridge adjacent MoS₂ and WS₂ nanosheets. To covalently link neighbouring flakes in a controlled and selective manner, yielding a hetero-network, a stepwise microfluidic-assisted strategy was developed, based on the findings described in D2.3. To understand the role of BDT in the MoS₂-WS₂ hetero-networks, a multiscale characterization of their films has been carried out.

2.2 Procedures

MoS₂ and WS₂ inks were prepared by sonicating pristine powders (Sigma Aldrich, purity > 99%) in N-Methyl-2-pyrrolidone (NMP) following a previously established procedure.^[3] Initial dispersions with a concentration of 20 mg/mL in NMP were subjected to sonication for 1 hour using a horn-tip sonicator (Sonics Vibra-cell VCX-750 ultrasonic processor) at 60% amplitude. The dispersions were then centrifuged at 3218 g for 1 hour using a Hettich Mikro 220R centrifuge. The supernatant was discarded to eliminate any potential contaminants originating from the starting powder. Subsequently, the sediment was redispersed in fresh NMP and sonicated under identical conditions for an additional 5 hours, yielding polydisperse stock dispersions. These dispersions underwent size selection of flakes through stepwise centrifugation. To remove the largest aggregates, the polydisperse stock was first centrifuged at 106.4 g for 90 minutes, with the sediment retained for future exfoliation. The supernatant was then further centrifuged at 425 g for 90 minutes to separate smaller flakes, which were finally redispersed in isopropanol (IPA).

The hetero-networks were fabricated using a custom-made microfluidic setup, including a chamber (Figure 1a) with an internal volume of 12 μ L, coupled with a peristaltic pump (Heidolph Hei-Flow Precision 01). The flow rate was maintained at a constant 0.6 mL/min throughout the process. To prevent aggregation of flakes and subsequent clogging, a tube with a diameter of 0.8 mm was employed. To form a uniform network, IPA dispersions of MoS₂ and WS₂ were alternated in the deposition process. Between each deposition step, a 50 mM solution of 1,4-benzenedithiol (BDT, Sigma Aldrich, \geq 99%) was circulated, as depicted in Figure 1b.

Si/SiO₂ substrates (15 \times 15 mm²) were thoroughly rinsed with acetone and 2-propanol to eliminate any potential contaminants. The surface of the substrates was then activated via UV/ozone treatment (NovaScan, Digital UV/Ozone System) for 20 minutes. To improve wettability, the substrates were subsequently immersed in a 1% solution of 3-(aminopropyl)triethoxysilane (APTES, Alfa Aesar, 98%) in water for 30 minutes. Separate dispersions of MoS₂ and WS₂ in isopropanol (IPA) were prepared at a concentration of 0.5 mg/mL and sonicated for 30 minutes in an ice bath.

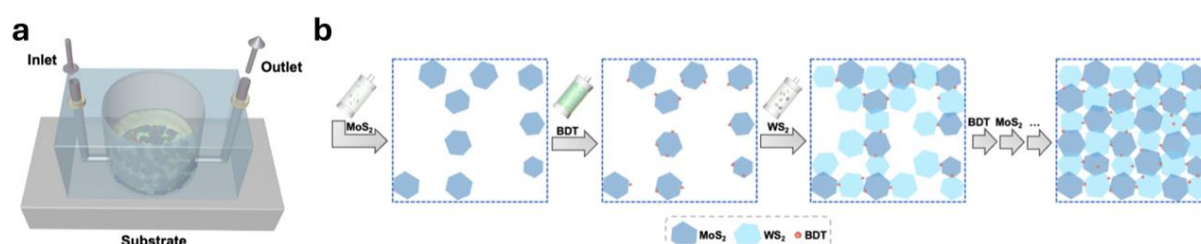


Figure 1. Microfluidic-assisted synthesis. (a) Schematic illustration of the microfluidic setup. (b) Schematic top-view of the stepwise growth of the lateral hetero-network fabricated using MoS_2 , BDT and WS_2 building units.

The stepwise growth of the hetero-networks was analyzed by both scanning electron microscopy (SEM) and electrochemical impedance spectroscopy (EIS). For EIS measurements, films were grown on custom-made electrodes, which were patterned onto n-doped standard Si/SiO₂ substrates (oxide thickness: 90 nm, substrate size: 15 × 15 mm) using maskless photolithography (Microtech LW405B laser writer) with AZ1505 photoresist and MIF726 developer. The channel length and width were both 10 μm. Subsequently, 3 nm of Cr and 40 nm of Au were thermally evaporated sequentially in a high-vacuum environment using a Plassys MEB 300 system, followed by sonication-assisted lift-off in acetone. An Olympus BX51 optical microscope was adopted to assess the quality of the lift-off process. Furthermore, the films were investigated by TAS (using a home-built pump-probe setup) and electrical measurements based on FETs. The FETs characteristics were measured using a source meter (Keithley 2636A) at room temperature under into a nitrogen-filled glovebox. A Pt wire was employed as the gate electrode, and a drop of 1-ethyl-3-methylimidazolium bis(trifluoromethylsulfonyl)imide (EMI-TFSI), TCI Chemicals, served as the ionic liquid gate dielectric. Thin films for electrical characterization were fabricated on bottom-contact n-doped Si/SiO₂ substrates (15 × 15 mm; Fraunhofer IPMS), with thermally grown 230 nm thick SiO₂ with interdigitated Au electrodes spaced at 2.5 μm and a channel length of 10 mm.

2.3 Data Analysis

In general, OriginLab software was used to carry out data analysis. In contrast, EIS data was analysed with the software NOVA, Metrohm Autolab. It also worth noting that, to account for spectral shifts in the excited state signals, the transient absorption (TA) spectra were fitted using a combination of 1, 2, or 3 Gaussians at each pump-probe delay time to track the peak shifts. Kinetic traces for each excitonic feature were extracted by identifying the maximum $\Delta T/T$ value at the wavelength determined from the Gaussian fitting, which allowed for the correction of spectral shifts. The resulting kinetics were modeled using a biexponential decay function: $\Delta T/T = A_0 + A_1 e^{-t/\tau_1} + A_2 e^{-t/\tau_2}$, where t denotes the pump-probe delay time, A_i represent the decay component amplitudes, τ_i are the corresponding lifetimes, and the average lifetime (τ_{ave}) was determined as the amplitude-weighted mean of the fast and slow decay components.

3 Results & Discussion

3.1 Results

The stepwise microfluidic-assisted strategy discussed in this report represents a feasible solution-processed approach to build cross-linked hetero-networks with high control and selectivity. Structural defects at the edges of TMDs are exploited to preferentially promote in-plane heterojunction formation by covalently bridging the flakes with dithiolated molecules. The morphology of the hybrid MoS₂–WS₂ heterostructure was characterized using scanning electron microscopy (SEM) and atomic force microscopy (AFM). To optimize the formation of a smooth solution-processed film, optical and SEM analysis was employed to track the arrangement of the nanosheets after each LPE TMD deposition step. It is noteworthy that the ~70% coverage of the interconnected film represents the best compromise between heterojunction formation and thickness (Figure 2a, b), as further deposition of either MoS₂ or WS₂ nanosheets would induce physisorption-driven vertical growth due to the overlap of flakes (Figure 2c), as the sulfur vacancies become less accessible in the densely packed coating. The smoothness of the solution-processed lateral hetero-network was further confirmed through AFM (Figure 2d).

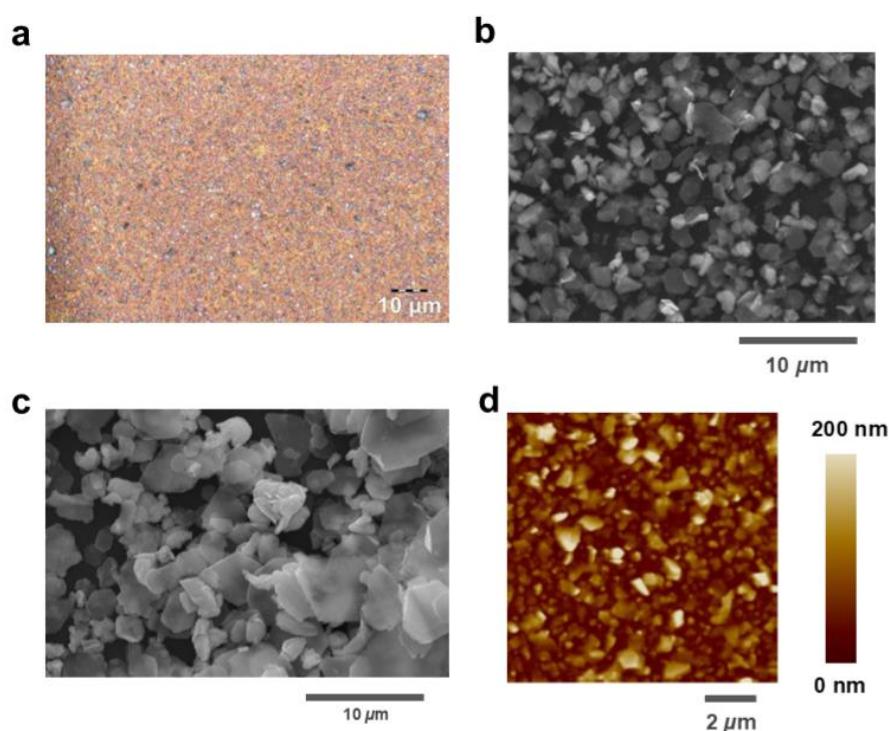


Figure 2. Network imaging. Optical (a) and SEM (b) images of a film based on the MoS₂-BDT-WS₂ hetero-network after optimization of the microfluidic process. (c) SEM image of a hetero-network after additional deposition steps exceeding the optimization threshold, showing aggregation and random vertical stacking. (d) AFM topographical image on a randomly selected area of the hetero-network.

To investigate the synergistic effect of using dithiolated molecules to drive the development of the heterostructure through preferential in-plane growth, as well as to facilitate the formation of

percolation pathways, EIS was employed. As shown in Figure 3a, a 2-electrode electrochemical cell was used for in situ EIS measurements. The growing heterostructure on patterned interdigitated electrodes, fabricated on APTES-modified Si/SiO₂ substrates, acts as a barrier to ionic conductivity (Figure 3b), which is initiated by applying a fixed sinusoidal voltage across the system. As the 2D assembly progresses, the ionic conductivity between the electrodes is hindered. EIS measurements revealed a significant increase in impedance after each TMD deposition step (Figure 3c), providing a real-time gauge to track the stepwise film formation via the microfluidic approach. The results indicate that larger planar coverage within the interdigitating electrodes is achieved due to the BDT-linking effect between adjacent flakes, promoting the lateral growth. To confirm the critical role of bidentate molecules in assembling the in-plane hetero-network, EIS was benchmarked after each MoS₂ and WS₂ deposition without BDT as an intermediate process. The spectra did not show any significant changes with increased TMDs loading, indicating partial and uneven surface coverage between the interdigitated electrodes (Figure 3d). A standard Randles equivalent circuit was used to fit the Nyquist plots extract the charge transfer resistance (R_{ct}), which represents the resistance to ionic conduction at the electrolyte-electrode interface. The architecture incorporating the cross-linked MoS₂–WS₂ hetero-network, mediated by BDT, exhibits a substantial increase in R_{ct} , along with the in-plane growth of the network (Figure 3e). In contrast, the deposition of nanosheets without any molecular linker resulted in minimal R_{ct} variation, consistent with an irregular and sparse coating of MoS₂ and WS₂ flakes.

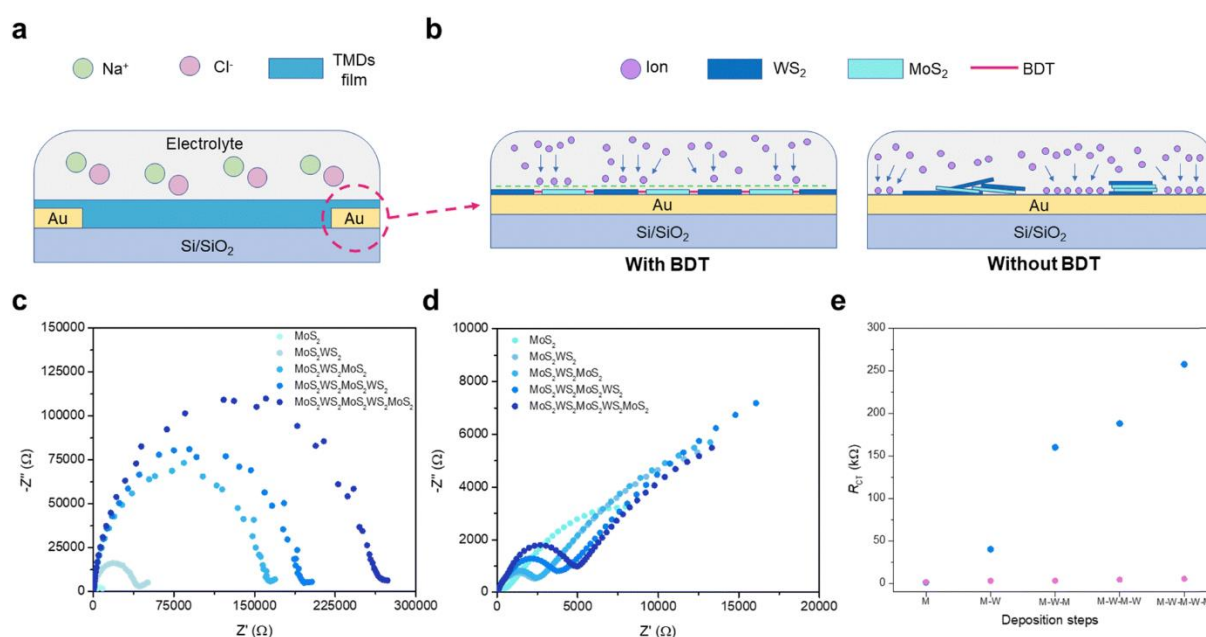


Figure 3. EIS tracking over the film growth. (a) Schematic illustration of the 2-electrode electrochemical cell. (b) Schematics of TMDs network acting as a barrier to ionic conductivity with (left) and without BDT as molecular linker (right). Nyquist plots evolution (c) upon BDT treatment between each MoS₂ and WS₂ step and (d) in absence of BDT. (e) R_{ct} comparison as a function of 2DMs deposition for networks with and without BDT, displayed in blue and purple, respectively.

To reveal the role of BDT in inducing changes in the overall photophysical features of the synthesized MoS₂–WS₂ hetero-networks, TAS analysis was carried out. The TA spectra of the hetero-network

exhibit typical excitonic signals arising from its components, such as the A-exciton (X_A) and B-exciton (X_B) from MoS_2 , and the X_A from WS_2 (from 550 nm to 725 nm), as shown in Figure 4a. For both pristine and BDT linked networks, the peaks corresponding to each exciton shifted spectrally at increasing pump–probe delay time, with each exciton in the pristine materials exhibiting a blue shift as their bandgaps returned to their ground-state values (Figure 4b). This behaviour was similar for the X_A of MoS_2 in the BDT-linked hetero-network (Figure 4c). In contrast, the trend was the opposite for the X_A of WS_2 (Figure 4d).

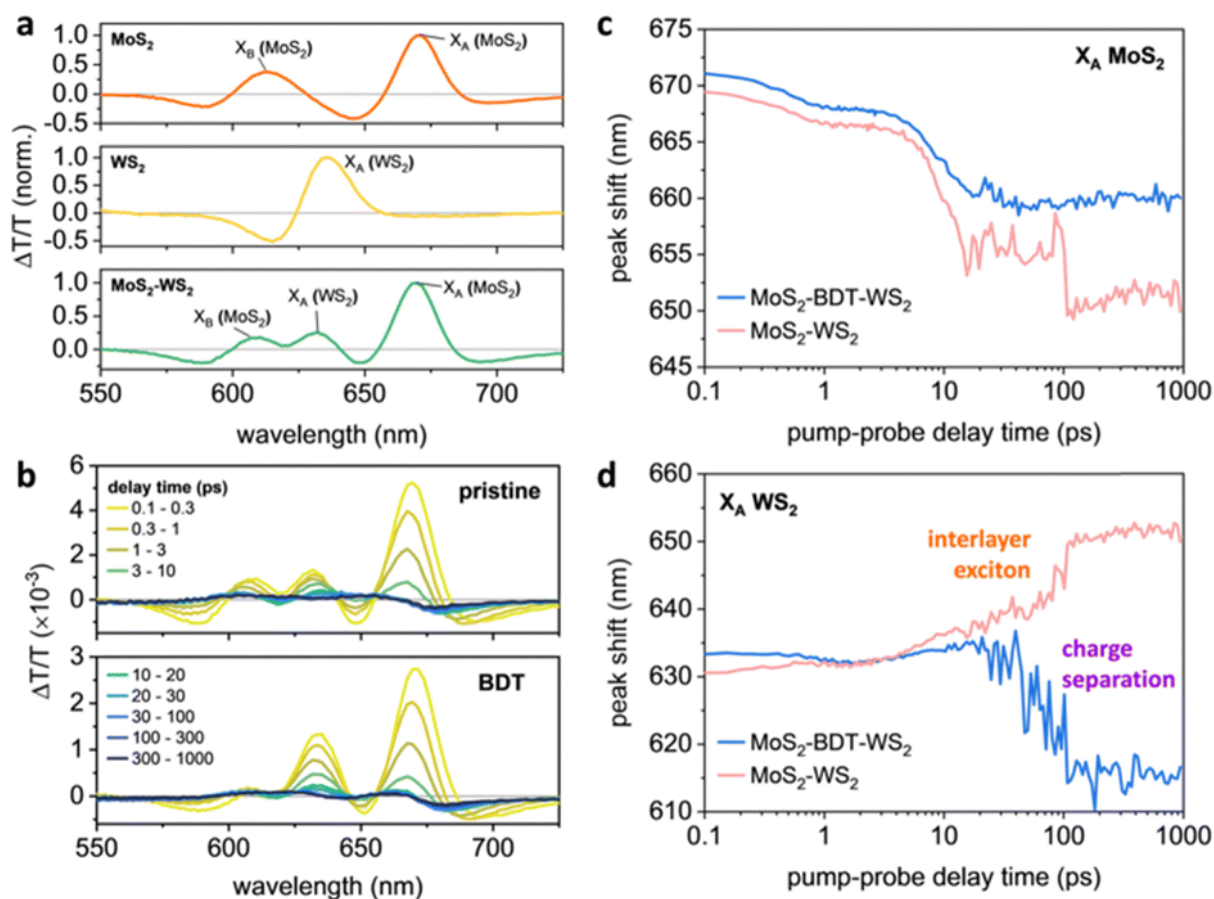


Figure 4. TAS analysis. (a) TA spectra of pristine MoS_2 , WS_2 , and $\text{MoS}_2\text{-WS}_2$ films averaged over pump–probe delay times of 0.1–0.3 ps. (b) TA spectra of $\text{MoS}_2\text{-WS}_2$ films, fabricated with or without BDT, averaged averaged over the pump–probe delay times listed in the legend. Peak shifts for (c) X_A of MoS_2 ; (d) X_A of WS_2 in the $\text{MoS}_2\text{-WS}_2$ films, with or without BDT, as determined from Gaussian fits.

For the blend without BDT, the X_A feature of WS_2 exhibited a red shift with increasing pump–probe delay times, indicating a narrowing of the WS_2 bandgap due to the formation of a long-lived interlayer exciton between MoS_2 and WS_2 , which is characteristic of vertical heterostructures.^[4] In contrast, for the BDT-linked hetero-network, the X_A characteristic in WS_2 blue-shifted back to its ground-state value within approximately 100 ps, further suggesting a distinct architecture with preferential in-plane assembly. Here, the rapid blue shift of X_A indicates the absence of tightly bound interlayer excitons, implying that the BDT-linked heterostructures facilitate faster charge separation. Further evidence was supported by the faster relaxation dynamics of WS_2 's X_A in the BDT-linked hetero-networks compared to the unlinked counterpart (Table 1).

Table 1. Summary of fits of kinetic traces.

Sample	Species	A ₀ (%)	A ₁ (%)	t ₁ (ps)	A ₂ (%)	t ₂ (ps)	t _{ave} (ps)
MoS ₂	X _A (MoS ₂)	4.40	30.22	0.490	65.38	2.99	2.10
MoS ₂ -BDT-MoS ₂	X _A (MoS ₂)	4.10	53.79	0.968	42.10	3.67	2.06
MoS ₂ -WS ₂	X _A (MoS ₂)	3.06	36.14	0.626	60.79	2.82	1.94
MoS ₂ -BDT-WS ₂	X _A (MoS ₂)	2.09	41.64	0.618	56.26	3.30	2.11
WS ₂	X _A (WS ₂)	5.97	41.00	0.805	53.03	7.08	4.09

The investigation of the electrical characteristics of the fabricated BDT-linked MoS₂-WS₂ hetero-networks was carried out on proof-of-concept bottom-contact, top-gated FETs. As shown in Figure 5a, the transfer characteristics of the cross-linked MoS₂ and WS₂ networks displayed *n*-type and ambipolar behaviour, respectively. The hetero-networks exhibited an *n*-type conduction, because only when both MoS₂ and WS₂ components are biased at ON state, the overall channel is turned ON.

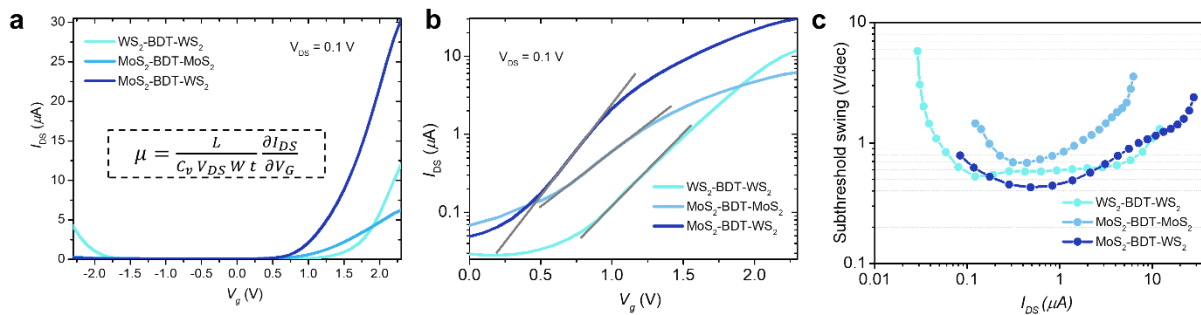


Figure 5. Electrical characteristics. (a) Transfer curves for BDT-linked networks. The equation for calculating the field-effect mobility (μ_{FE}) is shown in the inset. (b) Subthreshold slopes obtained from logarithmic-scale current characteristics of cross-linked networks. (c) Subthreshold swing (SS) as a function of drain-source current.

Moreover, FETs based on hetero-network exhibit lower threshold voltage, higher ON/OFF current ratio and increased mobility than homo-networks (Table 2).

Table 2. Mean values and standard deviation of key parameters calculated from the FETs based on BDT networks.

Film	μ_{FE} (cm ² V ⁻¹ s ⁻¹)	I _{ON} /I _{OFF}	V _{th} (V)	SS (V dec ⁻¹)
MoS ₂ -BDT-MoS ₂	(2.1 ± 0.2) × 10 ⁻²	(1.0 ± 0.1) × 10 ²	1.2 ± 0.2	0.63 ± 0.09
WS ₂ -BDT-WS ₂	(7.6 ± 0.1) × 10 ⁻²	(2.6 ± 1.3) × 10 ²	1.7 ± 0.1	0.56 ± 0.02
MoS ₂ -BDT-WS ₂	(1.6 ± 0.4) × 10 ⁻¹	(5.7 ± 2.0) × 10 ²	1.5 ± 0.2	0.31 ± 0.16

It worth noting that μ_{FE} values obtained from single flake-thick hetero-networks match state-of-the-art mobilities of LPE-based TMD films, which are typically 10²-10³ nm-thick.^[2,3] Hence, in-plane conductivity in the synthesized networks is maximized at reduced thickness by cross-linking nanosheets through their edge defects.

To estimate the trap density (D_{it}) in the networks, the slope of the transfer curves of the FETs were analysed (Figure 5b) and SS extracted (Figure 5c). The hetero-networks exhibited D_{it} of $3.4 \times 10^{14} \text{ V}^{-1} \text{ cm}^{-2}$, being lower than the BDT-homo-networks with MoS_2 and WS_2 ($8.0 \times 10^{14} \text{ V}^{-1} \text{ cm}^{-2}$ and $4.4 \times 10^{14} \text{ V}^{-1} \text{ cm}^{-2}$, respectively).

3.2 Contribution to project (linked) Objectives

The results of this deliverable contributed to different specific objectives of 2D PRINTABLE. The versatile synthetic strategy for hetero-networks, the multiscale characterization (i.e. EIS, TAS, electrical measurements) and proof-of-concept device benchmarking provide core units for objectives in WP3, as well as WP4, WP5 and WP6, as listed below:

- O3.2: "Demonstration of printed heterostructures using >20 different combinations of 2D materials."
- O4.2: "Establish basic and advanced characterization of nanosheet networks and heterostructures to assess morphology and nanosheet coupling."
- O4.3: "Develop new methodologies to characterize exfoliated nanosheets, in particular new materials and networks."
- O5.2: "Characterization and optimization of charge transport in printed networks and flake-level homostructures."
- O5.3: "Characterization and optimization of charge injection and transport in printed heterostructures."
- O6.2: "First demonstration of operational all-printed, all-nanosheet PV cells (PCE>10%) and LEDs (EQE>10%)."

3.3 Contribution to major project exploitable result

This deliverable contributed to reach different project tasks, such as the formation of bulk heterojunction heterostructures and provide a feasible strategy for the fabrication of a large number of heterostructures with distinct properties based on defect-engineering. Moreover, this deliverable will contribute to reach tasks in other WPs (i.e. T 4.4, T 5.2).

4 Conclusion and Recommendation

In conclusion, we have demonstrated the fabrication of cross-linked networks (both homo- and hetero-networks) based on defect-engineering. Chalcogen vacancies in TMDs, such as edge-sulfur vacancies in MoS_2 and WS_2 , have been exploited to link adjacent flakes through dithiolated π -conjugated molecules. The resulting cross-linked hetero-networks displayed distinct photophysical properties compared to conventional blends, as typical tightly bound excitons are suppressed, promoting faster charge separation. Furthermore, hetero-networks exhibited superior field-effect mobility due to a reduced trap density, resulting from the formation of heterojunctions. The approach described in D3.2 for assembling heterostructures from 2DMs inks is versatile and can be extended to other materials, using bidentate linkers tailored to the intrinsic defectivity of 2DMs beyond TMDs. The results of this deliverable offer many opportunities for progress in other WPs of 2D PRINTABLE.

5 Risks and interconnections

5.1 Risks/problems encountered

Risk No.	What is the risk	Probability of risk occurrence ¹	Effect of risk ¹	Solutions to overcome the risk
WP3.1	Aggregation can occur during the microfluidic process.	3	1	Tailor equipment tools (i.e. pipe size), wash between each deposition step and dilute the dispersion/solution

¹⁾ Probability risk will occur: 1 = high, 2 = medium, 3 = Low

5.2 Interconnections with other deliverables

D3.2 is mainly interconnected with D2.3, as the latter served as a platform to develop the synthetic strategy of cross-linked networks. Furthermore, some findings described in the D3.2 report can also be exploited for D3.3 and D6.2.

6 Deviations from Annex 1

Not applicable

7 References

- [1] A. Gaetano Ricciardulli, C. E. Petoukhoff, A. Zhuravlova, A. G. Kelly, C. Ma, F. Laquai, J. N. Coleman, P. Samorì, *Mater. Horiz.* **2024**, *11*, 5614.
- [2] S. Ippolito, A. G. Kelly, R. Furlan de Oliveira, M.-A. Stoeckel, D. Iglesias, A. Roy, C. Downing, Z. Bian, L. Lombardi, Y. A. Samad, V. Nicolosi, A. C. Ferrari, J. N. Coleman, P. Samorì, *Nat. Nanotechnol.* **2021**, *16*, 592.
- [3] A. G. Kelly, T. Hallam, C. Backes, A. Harvey, A. S. Esmaily, I. Godwin, J. Coelho, V. Nicolosi, J. Lauth, A. Kulkarni, S. Kinge, L. D. A. Siebbeles, G. S. Duesberg, J. N. Coleman, *Science* **2017**, *356*, 69.
- [4] P. Rivera, J. R. Schaibley, A. M. Jones, J. S. Ross, S. Wu, G. Aivazian, P. Klement, K. Seyler, G. Clark, N. J. Ghimire, J. Yan, D. G. Mandrus, W. Yao, X. Xu, *Nat. Commun.* **2015**, *6*, 6242.

8 Acknowledgement

The author(s) would like to thank the partners in the project for their valuable comments on previous drafts and for performing the review.

Project partners:

#	Partner short name	Partner Full Name
1	TCD	TCD THE PROVOST, FELLOWS, FOUNDATION SCHOLARS & THE OTHER MEMBERS OF BOARD, OF THE COLLEGE OF THE HOLY & UNDIVIDED TRINITY OF QUEEN ELIZABETH NEAR DUBLIN
2	UNISTRA	UNIVERSITE DE STRASBOURG
3	UKa	UNIVERSITAET KASSEL
4	BED	BEDIMENSIONAL SPA
5	TUD	TECHNISCHE UNIVERSITAET DRESDEN
6	VSCHT	VYSOKA SKOLA CHEMICKO-TECHNOLOGICKA V PRAZE
7	UNR	UNIRESEARCH BV
8	UniBw M	UNIVERSITAET DER BUNDESWEHR MUENCHEN
9	EPFL	ECOLE POLYTECHNIQUE FEDERALE DE LAUSANNE

Disclaimer/ Acknowledgment



Copyright ©, all rights reserved. This document or any part thereof may not be made public or disclosed, copied or otherwise reproduced or used in any form or by any means, without prior permission in writing from the 2D-PRINTABLE Consortium. Neither the 2D-PRINTABLE Consortium nor any of its members, their officers, employees or agents shall be liable or responsible, in negligence or otherwise, for any loss, damage or expense whatever sustained by any person as a result of the use, in any manner or form, of any knowledge, information or data contained in this document, or due to any inaccuracy, omission or error therein contained.

All Intellectual Property Rights, know-how and information provided by and/or arising from this document, such as designs, documentation, as well as preparatory material in that regard, is and shall remain the exclusive property of the 2D-PRINTABLE Consortium and any of its members or its licensors. Nothing contained in this document shall give, or shall be construed as giving, any right, title, ownership, interest, license or any other right in or to any IP, know-how and information.

This project has received funding from the European Union's Horizon Europe research and innovation programme under grant agreement No 101135196. Views and opinions expressed are however those of the author(s) only and do not necessarily reflect those of the European Union. Neither the European Union nor the granting authority can be held responsible for them.